



MICRON AND SUB-MICRON AEROSOL SIZING WITH A STANDARD PHASE-DOPPLER ANEMOMETER

Gerhard Göbel, Thomas Wriedt* and Klaus Bauckhage

Department of Chemical Engineering, University of Bremen, Badgasteiner Str. 3, D-28359 Bremen, Germany

(First received 6 May 1997; and in final form 16 January 1998)

Abstract—In this paper the extended application range of the standard phase-Doppler anemometer (PDA) to particle diameters below the commonly accepted lower limit of about 5–10 μm is described. The problems that accompany measurements on smaller particles are small scattering cross-sections and ambiguous relations between the measured phase difference $\Delta\Phi$ and the particle diameter d .

A simple, but flexible optical set-up for the transmitting part of a standard PDA system, and a numerical algorithm, which allows careful data evaluation from ambiguous $\Delta\Phi(d)$ relations, help to manage these problems. Measurements on aqueous suspensions of micron and sub-micron sized dielectric and metallic monospheres, as well as on polydisperse aerosols, are presented and evaluated by means of the proposed algorithm. © 1998 Elsevier Science Ltd. All rights reserved

1. INTRODUCTION

Optical particle sizing is a major discipline of aerosol science. The main advantage of optical techniques compared with other techniques is their non-intrusivity. Phase-Doppler anemometry offers the additional advantage of simultaneous size and velocity information on individual particles. Spraying processes are thus a typical application field for the PDA technique.

All optical particle sizing techniques rely on the significant dependance of the light scattering process of a sphere from its diameter. This dependence changes when particle sizes are under investigation, that are comparable with, or even smaller than the wavelength of the incident light. This leads to a variety of difficulties, that limit the application range of a standard PDA. Additional effort is necessary to extend the lower limit of a standard PDA to diameters clearly below 10 μm , a size range of common interest in aerosol science. Examples therefore are given, e.g. by Hinds *et al.* (1982).

2. STANDARD PHASE-DOPPLER ANEMOMETRY

A PDA system in its most simple form is build up of two laser beams and two optical detectors. A schematic set-up of such a standard PDA system is depicted in Fig. 1. Commercial PDA systems (Dantec, Aerometrics) often employ a third detector to allow cross-validation of the individual results. Some work has been done on small-particle PDA with these more sophisticated set-ups. This work is briefly discussed below. Within this paper we restrict ourselves to the standard PDA system.

The performance of a standard PDA system is mainly determined by the properties of the beam configuration system (laser wavelength λ , power P , beam waist radius ω , and beam crossing angle θ), the optical detection system (off axis angles φ , elevation angles ψ , detector field of view Ω), and the particle (size, shape and refractive index $m = n + ik$). A particle which travels across the intersection volume of two incident laser beams simultaneously scatters the light of both beams. The frequencies of the scattered fields are Doppler shifted. Interference between both scattered waves on the detector aperture leads to a beat signal

* Author to whom all correspondence should be addressed.

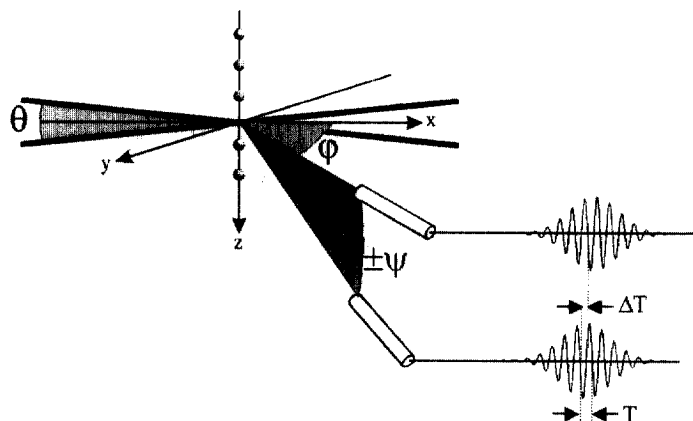


Fig. 1. Set-up scheme of a standard phase Doppler anemometer. Definition of beam crossing angle θ , elevation angles Ψ , and off axis angles φ . Though not obligatory, the detectors are commonly arranged symmetrically. The phase difference between both channels is defined as $\Delta\Phi = 2\pi \cdot \Delta T/T$.

(PDA burst). The beat or Doppler frequency f_D is a measure of the particle velocity. A time lag or phase shift between both detectors is determined by the size and the optical properties of the scattering particle. Light scattering computations yield the exact relation between this phase difference $\Delta\Phi$ and the particle diameter d . Spherical particle shape is assumed and Mie's scattering theory according to Bohren & Huffman (1983) is employed for that purpose.

PDA has been applied successfully, whenever the individual particles were spherical, homogeneous, and clearly larger than the laser wavelength λ . In those cases the scattered power is strong enough to be detected without difficulty. Furthermore, the relation between the measured phase difference $\Delta\Phi$ and the particle diameter d is linear. The exact relation can be obtained in close form from geometrical optics, as described, e.g. by Bauckhage (1988).

3. SMALL PARTICLE PHASE-DOPPLER ANEMOMETRY

For the classical scattering problem, defined by a spherical scatterer and a plane incident wave, Mie theory provides an exact solution in the form of a power series expansion, which has to be evaluated numerically. For the limiting case of a sphere clearly smaller (Rayleigh scattering) or clearly larger (geometrical optics) than the wavelength of light, approximative solutions exist in close form. Within these limiting cases all quantities of interest depend on the sphere diameter according to a power law. The Rayleigh behaviour can be obtained theoretically by means of a power series expansion of radial functions, which enter Mie's solution. The resulting behaviour of, e.g. the scattered intensity, $I \propto d^6$, is well known. The equivalent result for the phase $\Delta\Phi$ was found by Raszillier and Durst (1992), and is listed in Table 1 together with exponentials for other characteristic quantities of common interest in light scattering theory.

Table 1. Exponential n of a power law dependence $\propto d^n$ between sphere diameter d and phase difference $\Delta\Phi$, efficiency for scattering Q_s , and absorption Q_a , scattered intensity I , and $\langle \cos \varphi \rangle$, respectively, for the limiting cases of Rayleigh scattering and geometrical optics. The asymmetry parameter $\langle \cos \varphi \rangle$ is defined as the average value of the scattering cosine

Limiting case		$\Delta\Phi$	Q_s	Q_a	I_s	$\langle \cos \varphi \rangle$
Rayleigh: $d \ll \lambda$	$k = 0$	5	4	—	6	2
Rayleigh: $d \ll \lambda$	$k \neq 0$	3	4	1	6	2
GO: $d \gg \lambda$	any k	1	0	0/-	2	0

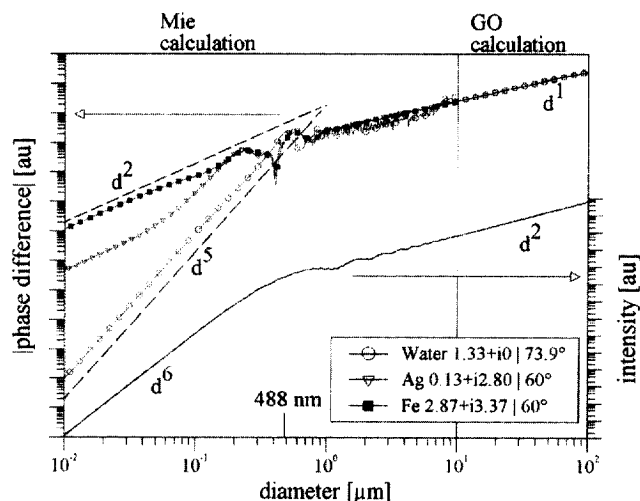


Fig. 2. Log-log diagram of phase difference $\Delta\Phi$ (left axis) and scattered intensity (right axis), both in arbitrary units, against particle diameter d for a laser wavelength of $\lambda = 488$ nm. Mie calculations have been performed for diameters $d < 10$ μm for H₂O, Ag and Fe. For $d > 10$ μm the geometrical optics results have been used. Indices of refraction and off axis angles ϕ are given in the legend for each material.

Most important for a PDA system are the scattered intensity I and phase difference $\Delta\Phi$. Figure 2 shows I and $|\Delta\Phi|$ against d in a log-log diagram for metallic and transparent spheres at a wavelength of $\lambda = 488$ nm. The diameter ranges from 0.01 μm up to $d = 100$ μm , thus covering both limiting branches. For diameters $d < 10$ μm Mie calculations have been performed. For $d > 10$ μm the result of the plain geometrical optics approach is depicted. General agreement between the Mie-calculation and the power law behaviour can be observed in all cases but one; while Raszilier predicted a d^3 dependance of the phase $\Delta\Phi$ for ideal conductors in the Rayleigh range, our Mie calculations clearly suggest $\Delta\Phi \propto d^2$ for metallic material. A d^3 dependence turns up only for even smaller diameters $d < 1$ nm. But this is a size range where the concept of bulk optical constants applied to individual particles loses its physical justification.

Two intrinsic problems of the PDA technique are obvious from Fig. 2 for particle diameters comparable to λ and below: firstly, there is a steady decrease of scattered intensity towards small diameters. For a fixed detector sensitivity and restriction of incident power to a reasonable amount, this fact is limiting the applicability of PDA as well as any other optical technique.

Secondly, the phase difference $\Delta\Phi$ decreases rapidly for small diameters. Though $\Delta\Phi(d)$ can be shifted to higher phase values by increasing the elevation angles Ψ of the detection system, a final minimum diameter can be obtained from a minimum resolvable phase difference. Actual minimum values depend on, e.g. set-up parameters and the detector sensitivity. As an example Naqwi (1994) gives $d \approx 100$ nm for transparent and $d \approx 20$ nm for conductive particles as the absolute theoretical PDA limit, assuming a minimum resolvable phase difference of 1°. In general, it can be stated, that conductive particles yield higher phase differences than transparent ones in the submicron range.

Two types of oscillations in the $\Delta\Phi(d)$ curve show up and can be a severe hindrance to a direct conversion of a measured phase to a sphere diameter. For transparent particles interference between refracted and reflected scattering components causes these oscillations for $d < 10$ μm . The oscillations can be reduced to a minimum mainly by Brewster reflection suppression, via smoothing by means of large detector apertures, asymmetric set-up types, or by means of a planar set-up according to Naqwi *et al.* (1991). These "high-frequency" oscillations cause an increasing source of uncertainty in the data evaluation process.

The other type of ambiguity can be observed from the small-particle limit for both transparent and absorbing particles. Here rather "low-frequency" oscillations are obvious

Table 2. Set-up information for the presented measuremental results. For suspension measurements the relevant angles inside the suspension cuvette are given. Note that the elevation angles of both detectors can differ. The state of polarisation was parallel with respect to the scattering plane for all measurements

Experiment	Off axis φ	Elevation Ψ	Beam crossing θ
Fig. 5, PS in H ₂ O	9°, 25°	+ 5.4°, - 6.6°	8.9°
Fig. 5, PS in H ₂ O	0°	+ 28.9°, - 26.2°	8.9°
Fig. 6, coated PS in H ₂ O	9°, 23°, 60°	+ 5.4°, - 6.6°	8.9°
Fig. 7, 9, 10, DEHS	20°, 66°	± 13.0°	11.8°

in the transition range between the exponential power law behaviour according to Table 1 and the linear $\Delta\Phi(d)$ relation. As will be shown below, this type of ambiguity can be reconstructed experimentally in detail. They have to be considered during phase to diameter conversion. A sophisticated data evaluation algorithm is introduced below.

Previous attempts to resolve the problems associated with small-particle PDA can be summarized as follows: Durst *et al.* (1996) favour the use of a non-linear optical component to reduce the wavelength of standard high-power cw-lasers by a factor of 2. This step is equivalent to an adaption of the measurement scale—here the wavelength of light—to the object to be measured. Naqwi and Zieme (1992) and Naqwi (1994) proposed a “joint probability density method” (JPDM) for simultaneous evaluation of at least two measured phase differences. Though practicable, this method requires a third optical detection and signal processing unit. v. Benzon *et al.* (1994) employed extreme set-ups to obtain unique phase values. For example they realized a beam crossing angle of nearly $\theta \approx 180^\circ$. Though successful, these proposals suffer from the fact, that they require either an extreme deviation from the standard PDA set-up, an extensive increase of hardware components (frequency doubling crystals, additional detection units), or sophisticated optical elements.

In contrary we propose an extension of the applicability range of a standard PDA by using only regular optical components and two optical detection units without additional hardware. The low-intensity problem is resolved by a novel transmitting optics concept for small particles, which allows a variable adjustment of the beam crossing angle θ and the beam waist radius ω . In order to enable PDA measurements in the presence of remaining ambiguities in $\Delta\Phi(d)$ a numerical algorithm for data evaluation is proposed and successfully applied to reference aerosols of known size.

4. DATA EVALUATION FROM AMBIGUOUS $\Delta\Phi(d)$

Ambiguous but moderate $\Delta\Phi(d)$ relations occur basically in two cases: they are inevitable for sphere diameters $d > 1 \mu\text{m}$, as obvious from Fig. 2. They also turn up for $d > 1 \mu\text{m}$ if the off axis angle corresponding to the Brewster angle is not accessible. Figure 3 elucidates the resulting problem by means of an imitated $\Delta\Phi(d)$ relation. An exemplary number density of diameters $q_0(d)$ is depicted, together with its corresponding number density of phase differences $q_0(\Delta\Phi)$.

Experimental data is available in form of number distribution $q_0^{\text{exp}}(\Delta\Phi_i)$ of phase differences. $\Delta\Phi_i$ is the centre value of class i . As obvious from Fig. 3 a different number of diameter ranges contributes to each phase class i . In addition, the width of each contributing diameter range depends on the local slope of $\Delta\Phi(d)$. Peaks occur in $q_0(\Delta\Phi_i)$ whenever the local slope of $\Delta\Phi(d)$ vanishes.

The presented algorithm is based on a suggestion of Schabel *et al.* (1994). The algorithm is limited to the evaluation of data from particle collectives that cover a significant diameter range of the ambiguous $\Delta\Phi(d)$. It is not capable of evaluating a single-phase measurement performed under an ambiguous $\Delta\Phi(d)$. Rather than trying to invert the measured q_0^{exp} distribution, we assume a parametric diameter distribution $q_0(d, \mathbf{p})$ and calculate its corresponding phase distribution $q_0^{\text{calc}}(\Delta\Phi_i)$ numerically with respect to the underlying

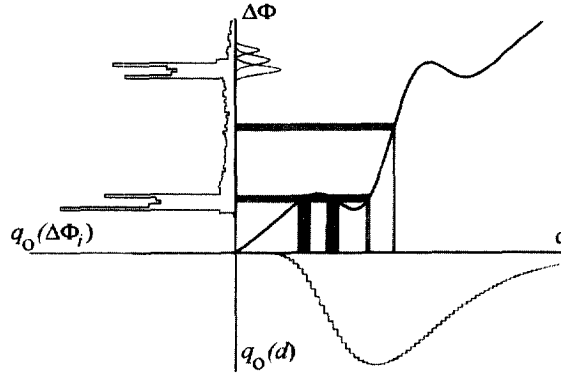


Fig. 3. Schema of the data evaluation algorithm for ambiguous $\Delta\Phi$. The I. quadrant shows an imitated $\Delta\Phi(d)$. A log-normal diameter distribution (number density) $q_0(d)$, depicted in the IV. quadrant, is transformed to a phase distribution $q_0(\Delta\Phi_i)$ (II. quadrant) by means of a statistical process.

$\Delta\Phi(d)$ relation. \mathbf{p} is the set of parameters necessary to characterize the real-size distribution $q_0(d)$. A log-normal distribution function with two parameters, d_0 and σ_{ln} , is usually sufficient for sprays and aerosols. The resulting $q_0^{calc}(\Delta\Phi_i)$ is rated against the experimental data $q_0^{exp}(\Delta\Phi_i)$ by calculating a square error sum:

$$\chi = \sum_{i=1 \dots N} \left(\frac{q_0^{exp} - q_0^{calc}}{q_0^{exp}} \Big|_{\Delta\Phi_i} \right)^2. \tag{1}$$

N is the number of classes. The above process is repeated with a changing set of parameters \mathbf{p} until χ reaches a predefined value. The choice of new parameters \mathbf{p} is performed by a random process based on principles of biological evolution, described by Hock & Rinderle (1980). The random step size in parameter space is determined by the history of the evolutionary process.

We calculate $q_0(d, \mathbf{p})$ on a random basis for each evolutionary step. The number of diameter events is chosen equal to the number of measured data points of the underlying experiment. For each randomly chosen diameter d the corresponding phase difference is taken from $\Delta\Phi(d)$. Before attachment to its phase difference class i we subject the individual phase difference value to a second random process, which accounts for a statistical error of the PDA system. This error is assumed to cause a Gaussian spreading of the real phase difference distribution. The Gaussian waist can be chosen to be an additional parameter of the evolutionary fitting process to obtain a measure for that statistical measurement error, whenever the experimental data contains sufficient information. This procedure is justified by the fact, that the significant peaks in $q_0(\Delta\Phi_i)$ due to vanishing slopes of $\Delta\Phi(d)$ are hardly observed that clearly in experiments. Furthermore, small phase difference values are often broadened into the negative range and turn up at the upper end of the size range ("ghost" events). Examples for both arguments will be given below.

Finally, we want to recall that the width and the mean of the particle size distribution under investigation have to be of such a kind that more than one single branch of the ambiguous $\Delta\Phi(d)$ is touched in order to achieve unique results from the evaluation algorithm. The size of extremely narrow ensembles (e.g. monospheres) cannot be recovered with this technique if $\Delta\Phi(d)$ is not unique.

5. TRANSMITTING OPTICS

In order to meet the demand for a small-particle PDA we designed the optical set-up depicted in Fig. 4. A radial diffraction grating (RDG, grid spacing $32 \mu\text{m}$, 70% total efficiency for 1st order beams) is used to split the incident laser beam. The main frequency of the Doppler signals can be shifted by means of rotation of the RDG in order to separate

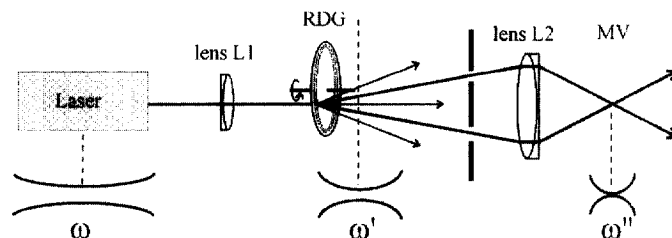


Fig. 4. Transmitting part of the optical set-up.

between opposite velocity components. This is of no importance for the application presented here. The diffracted beams are projected onto the location of the so-called measurement volume by means of a single achromat lens L2 ($f_{L2} = 160$ mm, $\phi_{L2} = 80$ mm). Thus, the beam crossing angle θ can be selected via the separation between the RDG and L2 according to the law of imagery. The maximum value is $\theta^{\max} = 26.4^\circ$.

Strong focusing of the Gaussian laser beam is necessary to yield a high incident power density. Therefore, a lens L1 is added to the optical path. By applying the imaging laws of Gaussian beams, which have been described by Self (1983), the position of both the laser and L1 are calculated in such a way, that the final position of the Gaussian beam waist ω''_0 coincides with the laser beam crossing position. Note that other than the lenses the grating is a diffractive optical element and therefore of no influence on the Gaussian behaviour of the beam. In general, the location of the beam waist after passing L1 is close to, but not identical with the position of the grating. As the divergence of a Gaussian beam is proportional to the reciprocal of the beam waist ω_0 , small displacements of the final waist position lead to large beam diameters at the position of the beam crossing, especially for strongly focusing set-ups.

The deviation between calculated beam waist diameters and experimental results recorded by means of a laser beam profiling system is typically less than 10%. For the measurements presented below we used a set-up with $f_{L1} = 150$ mm and $\omega''_0 \approx 10$ μm .

6. EXPERIMENTAL SET-UP

Our experimental set-up consists of the transmitting optics described in the previous section. It is fed by an air-cooled Ar-ion laser (100 mW at 488 nm, initial waist radius $\omega_0 \approx 0.41$ mm). All components are mounted on an optical bench.

Two independent photomultiplier tubes (PMT) with front lenses of $f_{\text{det}} = 100$ mm and a 52 mm circular aperture build up the optical detection system. Their PMT signals are band-filtered and amplified before digitization by means of a 30 MHz AD-board with a 12 bit dynamic range. Data evaluation is performed with an adopted FFT algorithm.

7. MEASUREMENTS ON MONOSPHERES

Measurements on suspensions of monodisperse spheres of precisely known size have been performed in order to reconstruct the “low-frequency” oscillations in the transition region from power law behaviour to linear $\Delta\Phi(d)$ relations. These experiments are similar to results published by, e.g. by Nawqi *et al.* (1991).

A cylindrical quartz flow cuvette (8 mm clear diameter, 74 mm length) was mounted to a squeezed tube pump. The flow was directed upward along the z -direction of Fig. 1. All angular set-up data has to be corrected for refraction at the air–glass–water interface.

We used transparent polystyrol spheres ($d < 2.0$ μm) and metal coated MF (melamin-resin) particles ($d < 10$ μm) from microparticles GmbH, i.g., Berlin, Germany. Mie calculations for coated spheres showed, that a metal layer of ≈ 50 nm is sufficient for a micron sized transparent sphere to be optically equivalent to a metal sphere without a core. The layer thickness was chosen accordingly by microparticles GmbH, i.g. Nickel

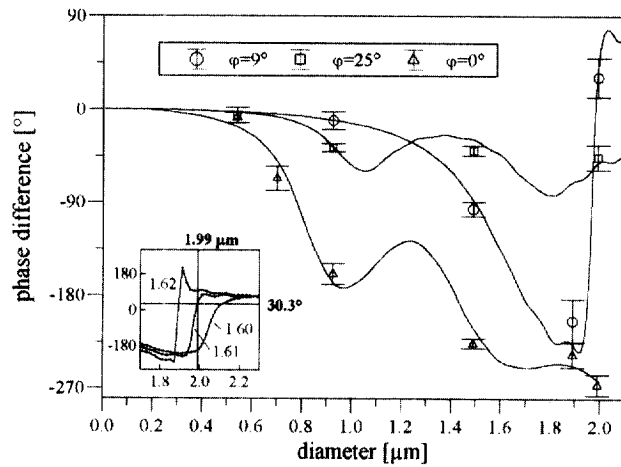


Fig. 5. Phase difference $\Delta\Phi$ against particle diameter d for PS spheres suspended in water. Measured values (data points) and Mie calculation (line). The abscissa is taken from the providers reference data. The bars represent the width of a Gaussian phase distribution fitted to the experimental data. The insert shows $\Delta\Phi(d)$ for $n = 1.600, 1.610,$ and 1.620 . Further information on the optical setup is given in Table 2.

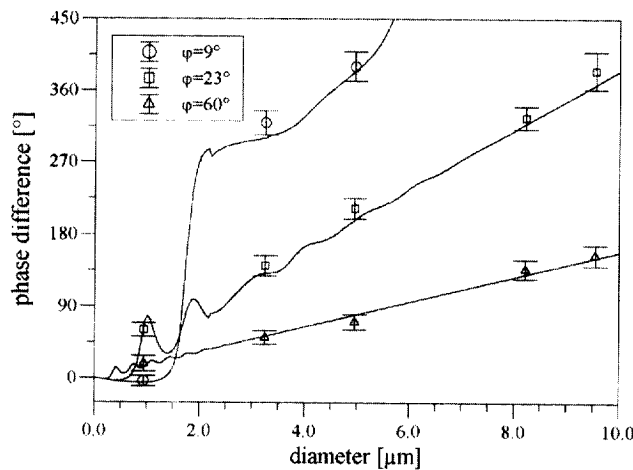


Fig. 6. Phase difference $\Delta\Phi$ versus reference particle diameter for various metal coated PS spheres suspended in water and three off axis angles ϕ . Again, reference diameter is taken from the provider, and the width of a Gaussian $q_0(\Delta\Phi)$ is depicted in form of a bar for each data point.

($m_{488} = 1.67 + i2.87$) and copper ($m_{488} = 1.13 + i2.45$) have been used as layer metals.

In Fig. 5 measured phase differences $\Delta\Phi(d)$ are plotted against the reference sphere diameter d of the transparent particles for off axis angles 0 (planar set-up), 9, and 25° and parallel polarized incident light. Note that there is phase jump in $\Delta\Phi(d)$ for the 9°-set-up. The position of that jump is very sensitive to a variation of the refractive index. This is demonstrated by the insert of Fig. 5, where the $\Delta\Phi(d)$ relation is depicted for slightly different values of n . As we happen to hit this jump experimentally ($d_{ref} = 1.99 \pm 0.04 \mu\text{m}$, $\Delta\Phi = 30.3^\circ$), the refractive index of the polystyrol could be determined as $n_{488} = 1.610 \pm 0.002$.

The depicted bars represent the width of a Gaussian phase distribution, which has been adjusted to fit the experimental data. This width should be governed by the width of the diameter distribution σ_d , the local slope of $\Delta\Phi(d)$, but also by statistical measurement errors. Nevertheless, general agreement can be found.

Figure 6 shows the equivalent result for the metal coated spheres. As the complex refractive index is practically of no influence on $\Delta\Phi(d)$, the results for both metals are

depicted in the same diagram. While in forward direction diffraction has some influence on $\Delta\Phi(d)$, reflection governs at larger off axis angles and $\Delta\Phi(d)$ is linear. Again, agreement between the experimental data and the Mie calculation can be observed.

8. MEASUREMENTS ON AEROSOLS

A Sinclair-La Mer condensation aerosol generator SLG 250 from *TOPAS*, Dresden, was employed as a source of monosized DEHS aerosols in the size range $0.1 \mu\text{m} < d < 5 \mu\text{m}$ ($\text{C}_{26}\text{H}_{50}\text{O}_4$, $\rho = 0.912 \text{ g cm}^{-3}$, $n_{488} = 1.455$). The size of these aerosols can be well described by a log-normal distribution $q(x, x_0, \sigma_{\ln})$ with two parameters x_0 and σ_{\ln} :

$$q(x, x_0, \sigma_{\ln}) = \frac{1}{\sqrt{2\pi}} \frac{1}{x\sigma_{\ln}} \exp \left\{ -\frac{1}{2} \left(\frac{\ln(x/x_0)}{\sigma_{\ln}} \right)^2 \right\}, \quad (2)$$

where x represents d or $\Delta\Phi$ for diameter distributions or phase difference distributions, respectively. Diameter selection was performed by adjusting the saturator temperature T_{sat} . The saturator represents that part of the SLG 250 where aerosol growth due to condensation takes place. From a calibration curve provided by *TOPAS* the aerodynamical diameter d_a of the aerosol can be obtained from T_{sat} to an accuracy of $\approx 0.2 \mu\text{m}$.

Two sets of measurements have been performed on that aerosols. While in a first step the optical set-up was chosen to yield a mostly linear $\Delta\Phi(d)$ relation ($\varphi = 66^\circ$), a second series ($\varphi = 20^\circ$) has been performed under a highly ambiguous $\Delta\Phi(d)$ with data evaluation according to the algorithm described above. Thus, the performance of the evaluation algorithm could be rated on an ambiguous $\Delta\Phi(d)$ system without the additional disturbance which inevitably accompanies PDA measurements on particles smaller than the DEHS aerosols.

Figure 7 shows the results of a measurement series performed under an off axis angle of $\varphi = 66^\circ$ for parallel polarization. This is close to the Brewster angle of the DEHS aerosol material. T_{sat} was varied from 140 to 240°C . The center values $\Delta\Phi_0$ of log-normal phase distributions q according to equation (2) are depicted against the aerodynamical diameter $d_a(T_{\text{sat}})$. The width σ_{\ln} of each distribution is again visualized by the vertical bars in Fig. 7. The bars delimit a e^{-1} decrease of a log-normal $q(x)$ with respect to the maximum value:

$$x_{\pm} = x_{\text{max}} e^{\pm\sqrt{2}\sigma_{\ln}}; \quad x_{\text{max}} = x_0 e^{-\sigma_{\ln}^2}. \quad (3)$$

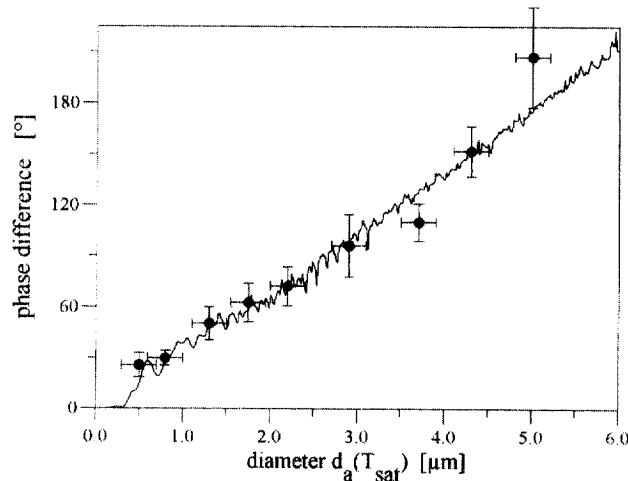


Fig. 7. Experimental results for aerosol measurements at Brewster's angle. The $\Delta\Phi_0$ of a log-normal phase distribution fitted to measured phase differences is plotted against the aerodynamical diameter $d_a(T_{\text{sat}})$. The horizontal bars are uncertainties of d_a while the vertical bars represent the e^{-1} values $\Delta\Phi_{\pm}$ according to equation (3) of the log-normal phase distribution.

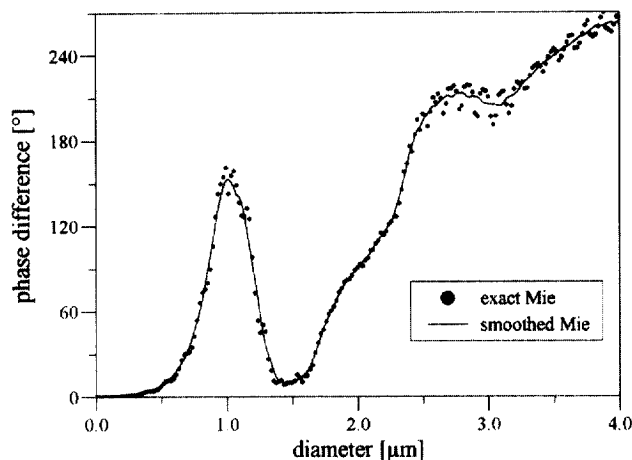


Fig. 8. $\Delta\Phi(d)$ for the DEHS system at an off axis angle of $\phi = 20^\circ$. Further, set-up information is given in Table 2. The data points represent the exact Mie calculation. We used the smoothed curve (line) for data evaluation.

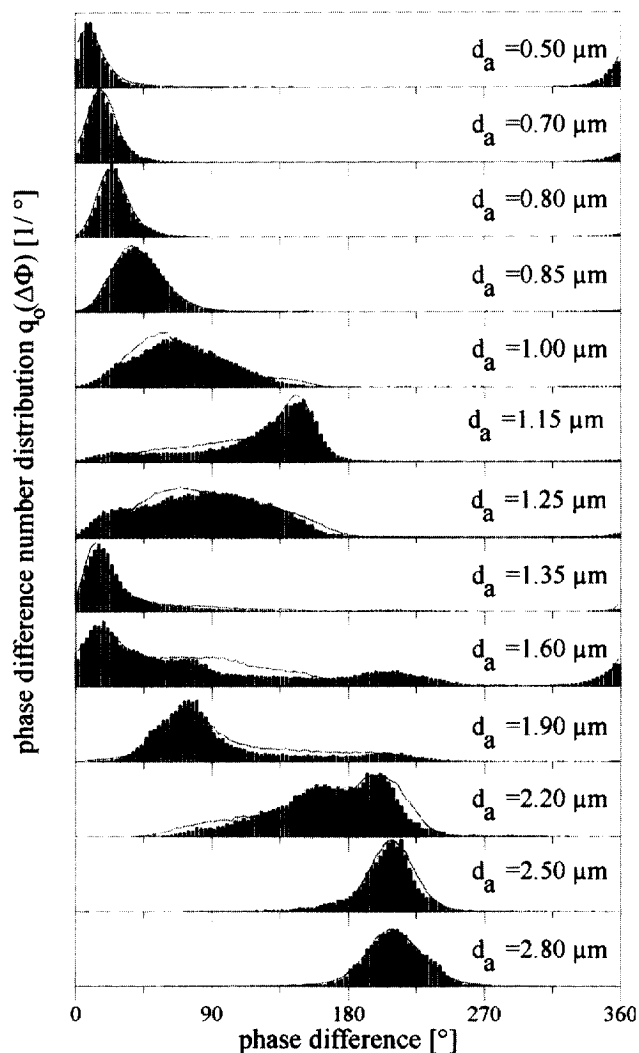


Fig. 9. Measured number density of phase difference $q_0(\Delta\Phi)$ against phase difference $\Delta\Phi$ for various saturator temperatures T_{sat} and corresponding aerodynamical diameters $d_a(T_{sat})$. While the histograms represent the measured distributions the solid lines are the result obtained by our data evaluation algorithm. The numerical data is listed in Table 3.

Table 3. Numerical data of the aerosol measurement series at 20° off axis angle. Saturator temperature T_{sat} , the corresponding aerodynamical diameter d_a , and the resulting data— d_0 and σ_{in} of a log-normal $q_0(d)$, and the Gaussian broadening width σ_g —are given

	# 1	# 2	# 3	# 4	# 5	# 6	# 7	# 8	# 9	# 10	# 11	# 12	# 13
T_{sat} (°C)	140	150	155	160	165	170	175	180	185	190	195	200	205
d_a (μm)	0.50	0.70	0.80	0.85	1.00	1.15	1.25	1.35	1.60	1.90	2.20	2.50	2.80
d_0 (μm)	0.516	0.605	0.658	0.732	0.806	1.01	1.24	1.39	1.63	2.03	2.42	2.88	2.92
σ_{in}	0.215	0.073	0.070	0.066	0.090	0.149	0.104	0.101	0.256	0.141	0.100	0.084	0.104
σ_g [°]	7.2	8.0	7.2	9.4	6.1	7.8	18.5	6.5	13.2	14.8	14.3	13.0	15.3

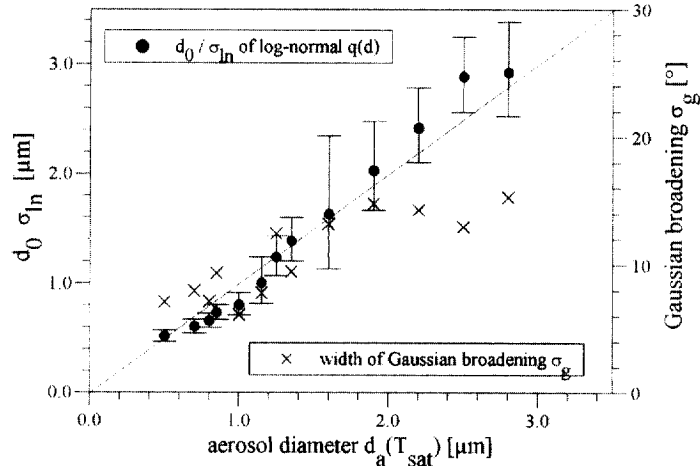


Fig. 10. Diameters d_0 and width σ_{in} of the data evolution results (●) vs aerodynamical diameter $d_a(T_{\text{sat}})$. The vertical bars represent the e^{-1} diameters of the log-normal diameter distributions. Also depicted is the result for the width of the Gaussian phase broadening σ_g (right axis). For reasons of clarity we refrained from depicting the uncertainty σ_d of the aerodynamical diameter $d_a(T_{\text{sat}})$.

The experimental results for the phase differences are in general agreement with the phases according to the Mie curve. Similar aerosol measurements under a quite smooth and unique $\Delta\Phi(d)$ have been published by Naqwi *et al.* (1996).

The second series of measurements was performed at an off axis angle of $\varphi = 20^\circ$, again for parallel polarization. Figure 8 shows the $\Delta\Phi(d)$ relation. Its shape is strongly influenced by diffracted components. By increasing the saturator temperature from 140 to 205°C we were able to scan a relatively narrow diameter distribution (geometric standard deviation < 1.15) through the ambiguous $\Delta\Phi(d)$. The resulting number distributions of phase differences $q_0(\Delta\Phi_i)$ are depicted as histograms in Fig. 9. Starting from small diameters d_0 an increase of the width of $q_0(\Delta\Phi_i)$ due to the increasing slope of $\Delta\Phi(d)$ can be seen. Furthermore, the first maximum of $\Delta\Phi(d)$ at $d \approx 1.0 \mu\text{m}$ and the second one at $d \approx 16 \mu\text{m}$ are clearly transformed into limiting phase difference values. Here the shape of the depicted $q_0(\Delta\Phi_i)$ is strongly dominated by $\Delta\Phi(d)$ rather than by $q_0(d)$. But as mentioned before, these limiting values are smoothed by a Gaussian broadening of measured phase differences. This is also obvious from the small diameter measurements. Here the broadening leads to negative $\Delta\Phi$, which are 360° shifted towards large $\Delta\Phi$. To account for that effect we are encouraged to apply a Gaussian broadening to the numerically obtained phase differences within our algorithm, as described above. A slightly smoothed $\Delta\Phi(d)$ (Fig. 8) was used to determine the parameters of a log-normal $q_0(d)$ according to equation (2) and the width of the Gaussian phase difference broadening σ_g from each measured $q_0(\Delta\Phi_i)$. The solid lines in Fig. 9 represent the best fitting $q_0(\Delta\Phi_i)$. All data are also listed in Table 3. Finally, all results are depicted in Fig. 10 against the aerodynamical diameter $d_a(T_{\text{sat}})$. The agreement between d_a and d_0 from our algorithm is good. The minor differences are similar to the

results from the 66° measurement. The measured phase differences are slightly underestimated for $d_a < 2 \mu\text{m}$, while they are a little to high above $2 \mu\text{m}$. A systematic source of deviation, e.g. in the calibration curve could be the reason. The width of the Gaussian broadening σ_g seems to increase with d_a , thus supporting a relative width rather than an absolute one. For $d_a > 2 \mu\text{m}$ σ_g is constant at $\approx 14^\circ$.

9. CONCLUSIONS

Within this work we are able to apply phase Doppler anemometry in its standard configuration to micron and sub-micron monospheres and aerosols. Down to diameters of $0.5 \mu\text{m}$ low scattered intensity is no serious problem even for moderate laser power if an appropriate transmitting system is employed. A simple optical set-up for that purpose was introduced.

Furthermore, we showed that some degree of ambiguity in the $\Delta\Phi(d)$ relations can be taken into account within data evaluation. This procedure can certainly not be transferred to any ambiguous situation. Instead, we have to recommend a careful consideration of the individual case.

A rigorous solution to all difficulties is not available. Application of the PDA technique to even smaller particles is principally possible, but will soon lead to solutions with high additional hardware requirements.

REFERENCES

- Bauchhage, K. (1998) The phase-Doppler-difference-method, a new laser-Doppler technique for simultaneous size and velocity measurements—part I. Description of the method. *Part. Part. Systems Charact.* **5**, 16.
- v. Benzon, H. H. and Buchhave, P. (1994) The phase-Doppler method applied to very small particles. *Part. Part Systems Charact.* **11**, 55.
- Bohren, C. F. and Huffman, D. R. (1983) *Absorption and Scattering of Light by Small Particles*. Wiley, New York.
- Durst, F., Melling, A. and Volkholz, P. (1996) Advantages of UV lasers in laser and phase Doppler anemometers for submicrometer particles. *8th Int. Symp. on Applications of Laser Techniques to Fluid Mechanics*, Lisboa, Portugal.
- Hinds, W. C. (1982) *Aerosol Technology*. Wiley, New York.
- Hock, A. and Rinderle, J. (1980) Zur Anwendung der Evolutionsstrategie auf Schaltungen der Nachrichtentechnik. *Frequenz* **34**, 208.
- Naqwi, A. and Ziemann, M. (1992) Extended phase Doppler anemometer for sizing particles smaller than $10 \mu\text{m}$. *J. Aerosol Sci.* **23**, 613.
- Naqwi, A., Durst, F. and Kraft, G. (1991) Sizing of submicrometer particles using a phase-Doppler system. *Appl. Opt.* **30**, 4903.
- Naqwi, A. (1994) *In situ* measurements of submicron droplets in electrosprays using a planar phase Doppler system. *J. Aerosol Sci.* **26**, 1201.
- Naqwi, A. (1994) Innovative phase Doppler systems and their applications. *Part. Part. Systems Charact.* **11**, 7.
- Naqwi, A., Menon, R. and Fingerson, L. M. (1996) An adaptive phase/Doppler system and its applications including particle sizing in submicron and nanometer ranges. *Exp. Fluids* **20**, 328.
- Raszillier, H. and Durst, F. (1992) The electromagnetic scattering problem of Laser-Doppler anemometry—Part I. Fluid investigation. *Part. Part. Systems Charact.* **9**, 105.
- Raszillier, H. and Durst, F. (1992) The electromagnetic scattering problem of Laser-Doppler anemometry—Part II. Particle investigation. *Part. Part. Systems Charact.* **9**, 186.
- Schabel, S., Doicu, A. and Ebert, F. (1994) Corrections of particle size distributions from PDA-measurements for continuous distributions less than $10 \mu\text{m}$. *7th. Int. Symp. on Appl. of Laser Tech. to Fluid Mechanics*, Lisboa, Portugal.
- Self, S. A. (1983) Focusing of spherical Gaussian beams. *Appl. Opt.* **22**, 658.